ICWE14
June 21-26, 2015 | Porto Alegre - Brazil
14th INTERNATIONAL CONFERENCE ON WIND ENGINEERING

Wind turbine and actuator disc wake: two experimental campaigns

Lorenzo E.M. Lignarolo[1], Daniele Ragni[1], Carlos J. Simão Ferreira[1], Gerard J.W. van Bussel
[1]Department of Aerodynamics Wind Energy Flight Performance and Propulsion, Faculty of Aerospace Engineering, Delft University of Technology, Delft, The Netherlands
email: L.Lignarolo@tudelft.nl D.Ragni@tudelft.nl C.J.SimaoFerreira@tudelft.nl G.J.W.vanBussel@tudelft.nl

ABSTRACT: The present paper is the summary of 3 years of research on the wake aerodynamics of horizontal axis wind turbine at Delft University of Technology, the Netherlands. In particular, the main results and the conclusions of two experimental campaigns are collected. The underlying research question is: how do the near-wake turbulent flow structures affect the re-energising of the far wake and to what extend is the actuator disc assumption valid for the representation of the near wake dynamics? In the first experiments, stereo particle image velocimetry is used for analysing the turbulent velocity field in the near and transition wake of a small two-bladed wind turbine model. The results showed the important role of the tip-vortex helix instability (*leapfrogging*) in the mixing process and in the re-energising of the wake. The tip-vortex instability and breakdown, in fact, give rise to a more efficient turbulent mixing. In the second campaign, the same measurement technique is used for acquiring data in the near wake of the wind turbine model and in the near wake of a porous disc, emulating the numerical actuator disc. The results show a good match velocity fields between wind turbine and actuator disc, but show a different turbulence intensity and turbulent mixing. The analysis suggest the possibility to extend the use of the actuator disc model in numerical simulation until the very near wake, provided that the turbulent mixing is correctly represented.

KEY WORDS: Tip-Vortex Instability; Wind Turbine Wake; PIV Experiments; Wake Turbulence; Actuator Disc.

1 INTRODUCTION

The persistence of the wake over a significant distance from the wind turbine in large clusters or arrays of rotors (as in wind farms) limits the energy performance of the entire farm [21], as well as inducing unsteady loads, noise and fatigue on the downwind turbines [20, 24]. In off-shore environment, where the atmospheric turbulence is lower than on-shore, wake effects become more important, due to the lower turbulent mixing [12]. Knowledge about the basic mechanisms behind the breakdown of the tip-vortices spiral-systems is particularly relevant in off-shore wind turbines to correctly estimate the extent of the near-wake region, dominated by strong and coherent flow fluctuations. The wake of a single rotor-blade consists of a continuous sheet of trailed vorticity due to the change in bound circulation along the blade span, which rolls up forming two concentrated tip and root vortices. These vortical structures determine a helical system, due to the combination of the rotational motion of the blade, the free-stream wind-flow and the velocity field induced by the vortex system itself. The stability properties of such a system of vortex filaments have been investigated by several authors (see the review work by [23]) and it has been shown that very often the tip-vortex helical filaments interact with each other (forming pairs of groups of three, depending on the number of blades in the rotor) anticipating the tip-vortex breakdown [4, 11, 23]. This phenomenon is normally referred to as *leapfrogging* of the tip-vortices. Moreover, the instability and breakdown of the helical system of vortices in the near wake is reported to affect the development of the turbulence in the far wake, where the mixing process between the inner and the outer flow regions occurs. Any design inducing an earlier instability and more effective mixing process will result in a more rapid recovery of the momentum defect, with benefits on the energy efficiency which can be maintained even with a lower spacing between turbines [23]. Only a few studies focus on the self-induced mixing of the wake ([9, 12, 22, 23, 25]). One of the main problems, which still remains open, is the quantification of the effect of the near-wake instability and the tip-vortex breakdown on the mixing process of the wind-turbine far-wake and, consecutively, on the wake re-energising [23]. Two opinions are found in scientific literature: [16] ascribes the missed energy recovery in the near wake to the *shielding* effect of the strong concentrated tip vortices, in contrast with previous studies, which tend to consider tip vortices as structures that enhance the mixing by entraining high-momentum fluid from the outer stream [10].

Due to this highly complex near-wake phenomenon, the numerical simulation of the near wake flow is problematic. The most common approach used to simplify the numerical simulation of the flow in a wind farm is to model the single rotors as stationary actuator discs. However, it is known from literature that this approach intrinsically misestimates the effects of flow turbulence, due to the absence of the blade flow and of its tip-vortex development and breakdown [3]. Consequently the mixing process across the wake interface and ultimately the rate at which the wake recovers the flow kinetic energy (wake

re-energising) is incorrectly modelled [20, 26]. As a matter of fact, currently in-use wind farm numerical models often struggle to accurately reproduce the flow within a wind farm. In particular, there are issues with the correct prediction of the power deficit at the second row of wind turbines, as the incoming flow develops from an atmospheric boundary layer to a wind farm canopy boundary layer [19]. For this reason, the wind energy community is working towards full-wake models, including a better representation of the near-wake flow induced by a more realistic modelling of rotor aerodynamics. Despite the popularity of this simplified numerical model, few experimental studies are available, which analyse the flow field in the wake of an actuator disc experimentally or numerically [2, 17, 22, 25], but a detailed high-resolution 2D measurement of the flow in the wake a porous disc, including velocity field and turbulence statistics, is currently not available.

The present paper collects the results of two extended experimental campaigns, in which the wake of a small-size wind turbine model and of a porous disc of the same diameter have been measured in controlled conditions with the Stereo Particle Image Velocimetry (SPIV) technique. In the first experimental campaign, the wake of the turbine alone has been considered. The study was focussed on addressing the following open questions in wind turbine wake aerodynamics:

1a) what are the most relevant turbulent structures for correctly modelling the kinetic energy transport in the wake?
1b) How does the pairwise instability of the tip-vortex helices in the near-wake affect the evolution of the turbulence and turbulent mixing in the far wake region?
1c) What is the role of the tip-vortices in the near-wake, i.e. do they inhibit or enhance the transport of kinetic energy?

In the second experimental campaign, the wake of a porous disc (emulating the numerical actuator disc) was compared with the wake of the same rotor considered in the first campaign. The general purpose was to highlight and to quantify the differences and similarities of the two models in the near wake region, characterised by the largest discrepancies, especially when in presence of *leapfrogging*. The study was focussed on addressing the following questions:

2a) How do the differences in the wind turbine and actuator disc near wake affect the physics of the wake flow?
2b) To what extend is the actuator disc assumption valid for the representation of the near wake dynamics?

The project is intended to provide the basis for understanding the origin of the limitations of the current wake models based on the actuator disc assumption.

The results of the first experimental campaign have been presented and discussed in depth in [13] and in [15]. The results of the second experiment have been discussed in [14]. The aim of this work is to give a critical interpretation of this experimental work and draw global conclusions.

2 METHOD

In this paper report only the analysis of the turbine and actuator disc wake in terms of mean-flow kinetic-energy transport and turbulence intensity. The former is an important quantity, which represent the amount of free-stream kinetic energy entrained inside the wake and is representative of the flow mixing in a particular region.

In the first campaign, velocity fields are acquired with stereo particle image velocimetry (SPIV), both randomly sampled and phase-locked with the turbine-blade motion. This allowed a statistical analysis of the mixing process of the wake, by applying a triple decomposition of the flow [18] as explained in [15] in mean flow, organised periodic motions and random turbulent fluctuations. This allowed to calculate the phase-average mean-flow kinetic energy flux [5, 6] as in Eq.(1):

$$\left\langle \widetilde{\Phi} \right\rangle = \bar{u}\left\langle \tilde{u}\tilde{v} \right\rangle \qquad \left\langle \Phi_s \right\rangle = \bar{u}\left\langle u_s v_s \right\rangle \tag{1}$$

where $\bar{u}$ is the time-average axial velocity $\langle \tilde{u}\tilde{v} \rangle$ and $\langle u_s v_s \rangle$ are the phase-locked Reynolds shear stresses due to periodic and random motions respectively (see [15] for detailed explanation). The phase-locked turbulence intensity $\langle TI \rangle$ is calculated as in [13] and shown in Eq.(2):

$$\langle TI \rangle = \frac{1}{U_\infty}\sqrt{\frac{1}{3}\sum_{i=1}^{3}\langle u_{s,i}u_{s,i}\rangle}^{\,2} \tag{2}$$

where U_∞ is the inflow velocity, the index i refers to the direction and is $i = 1,2,3$ respectively for the x-, y- and z-direction (axial, radial and out-of-plane) and the quantity $\langle u_{s,i}u_{s,i} \rangle$ represents the normal Reynolds stresses due to random motions. The analysis is performed for two rotational speeds, $\lambda = 6$ and $\lambda = 4.8$, where λ is the tip-speed ratio calculated as the ratio between the speed of the blade tip and the free-stream wind speed. In this paper, only the results for $\lambda = 6$ are reported, obtained with a rotational frequency of ω=113.1 rad/s and a free-stream velocity of 5.7m/s (see Table 1).

In the second campaign, velocity fields are acquired with SPIV with random sampling and a statistical analysis of the mixing process of the wake is performed calculating the time-average mean-flow kinetic energy flux as in Eq.(3):

$$\bar{\Phi} = \overline{u}\,\overline{u'v'} \tag{3}$$

without distinguishing between the contribution of the organised periodic motions and the random turbulent fluctuations. The time-average turbulence intensity $\overline{TI}$ is calculated as in [13] and shown in Eq.(2):

$$\overline{TI} = \frac{1}{U_\infty}\sqrt{\frac{1}{3}\sum_{i=1}^{3}\overline{u'_i u'_i}} \tag{4}$$

where the quantity $\overline{u'_i u'_i}$ represents the normal Reynolds stresses due to both periodic and random motions. The analysis is performed for only one tip-speed ratio λ = 6.97, obtained with a rotational speed ω=109.3rad/s and a free-stream velocity of 5.7m/s (see Table 1)..

2.1 Experimental set-up

2.1.1 Wind tunnel

Both the experiments have been conducted in the low-speed closed-loop Open-Jet Facility (OJF) wind tunnel located at the AWEP Department of Delft University of Technology. The OJF wind tunnel has an octagonal test section with an equivalent diameter of 3 m and a contraction ratio of 3:1, delivering a uniform stream with approximately 0.5% turbulent intensity up to 1 m from the nozzle and lower than 2% at 6 m from the nozzle exit. The flow is driven by a fan with an electrical engine of 500 kW and the temperature is kept constant by a heat exchanger which provides up to 350 kW of cooling power.

2.1.2 Wind turbine model

A two-bladed horizontal-axis wind-turbine with a 0.6 m diameter has been designed for an optimal tip-speed ratio $\lambda = \omega\, r/U_\infty = 6$ and a thrust coefficient $C_t = 0.89$. The wind turbine is operated at a free-stream wind velocity U_∞ = 5.7 m/s and U_∞ = 4.7 m/s in the first and second experimental campaign respectively, with a tip-speed ratio λ =6.00 and λ =6.97 respectively. At these conditions the maximum chord-based Reynolds number achieved is Re_{ct} = 100,000. A six-component balance is used for measuring the drag force on the turbine. For tip-speed ratio λ = 6.97 the thrust coefficient was C_t = 0.93. A detailed description of the wind turbine design can be found in [13].

2.1.3 Actuator disc model

The numerical abstraction of an infinitely thin circular region, where body forces extract momentum from the wind flow, can be reproduced in a wind tunnel via a porous disc which quickly dissipates the kinetic energy of the incoming flow into small-scale turbulence and, eventually, into heat [1, 2, 16, 17, 22]. A 0.6 m diameter porous disc is manufactured by stacking three layers of metal mesh with uniform porosity p = 60% in a sandwich structure between two additional meshes of very large porosity for fine-tuning the drag coefficient and flattening the underlying layers of fine mesh, as well as supporting and stiffening the whole structure. A disc with total porosity p = 32% and drag coefficient C_D = 0.93 (equal to the turbine's C_t = 0.93) is obtained. A disc of uniform porosity has been used, neglecting the distribution of loads on the WT's blades.

2.1.4 Stereoscopic particle image velocimetry

A stereoscopic PIV setup has been installed on a traversing system able to translate in 2D of about 1.2 m × 0.9 m. and to scan the flow field in a large portion of the wake. The required illumination is provided by a Quantel Evergreen Nd:YAG laser system with an average output of 200 mJ/pulse. Two LaVision Imager Pro LX 16 Mpix (4870 × 3246 px^2, 12 bits) with pixel pitch of 7.4 μm/px are used to acquire images with a field of view of 0.357×0.253 m^2 and 0.297×0.227 m^2 in the first and second campaign respectively. The velocity fields are obtained by stitching several fields of view. The general setup is shown in the schematic of Figure 1.

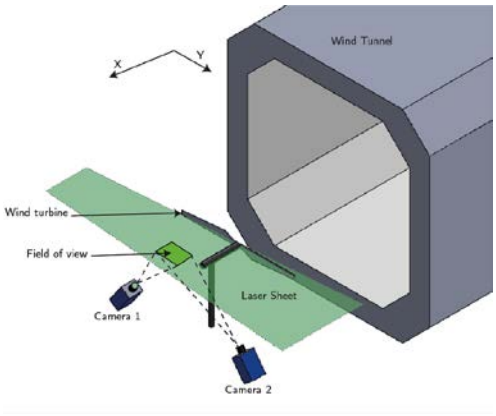

Figure 1. Wind tunnel schematic (from [13])

Table 1 summarises the experimental conditions for the two campaigns. The following sections contains a brief (partial) description of the results of the experiments.

Table 1. Experimental conditions of the two campaigns.

Parameters		**First campaign**	**Second campaign**	
		WT	**WT**	**AD**
Free-stream velocity	U_∞	5.7 m/s	4.7 m/s	4.7 m/s
Free-stream turbulence intensity	TI_∞	0.5%	0.5%	0.5%
Rotational frequency	ω	113.1 rad/s	109.3 rad/s	-
Reynolds (chord based) blade tip, $r/R = 1$	Re_{ct}	100,00	96,000	-
Reynolds (diameter based)	Re_D	228,000	188,000	188,000
Thrust coefficient (balance measurements)	C_t	0.89	0.93	0.93
Tip speed ratio	λ	6.00	6.97	-

3 RESULTS

3.1 First experimental campaign

Figure 2(top) shows the time-average (unconditioned sampling) and Figure 2(bottom) the phase-average (phase-locked sampling) axial velocity field for $\lambda = 6$. The leapfrogging location starts at $x/D \sim 1$. In the time-average field, this is visible in a localised increase of the shear layer thickness between $x/D \sim 1$ and $x/D \sim 2$. In the phase-average field, the single vortices are visible and the process of the leapfrogging is distinguishable: at $x/D \sim$ 1m two consecutive vortices start interacting and at $x/D \sim 1.5$ they are one on top of each other, after breaking down and diffusing after $x/D \sim 2$.

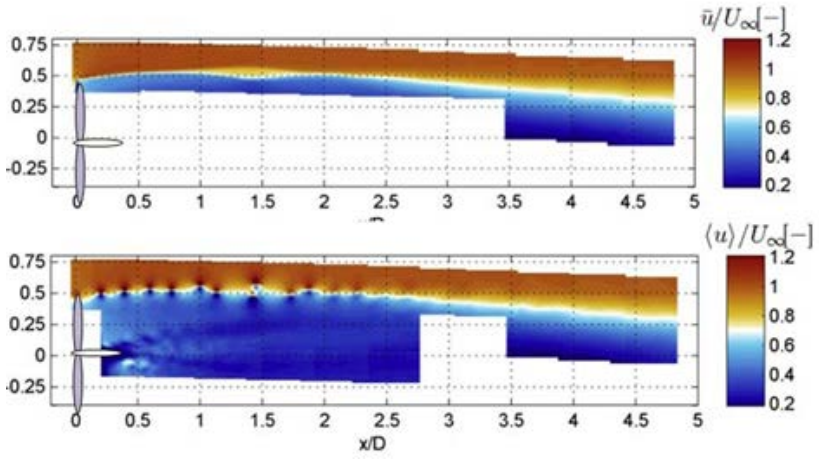

Figure 2. Unconditioned (top) and phase-locked (bottom) average axial velocity field in the wake of the WT in the first campaign (from [13])

Figure 3 shows the streamwise development of the phase-locked axial velocity field at 4 different radial locations (from [13]). The red dot indicates the location where two tip vortices have completed a 90 degree rotation around each other in the process of leapfrogging, here called “maximum leapfrogging”. Results show that the wake instability caused by the pair-wise interaction of the blade tip-vortices has a strong impact on the momentum deficit recovery of the wake, causing the wake re-energising happen right after the maximum leapfrogging location. It can be hypothesised that this happens by enhancement of the mixing process downstream of the tip-vortex helix instability.

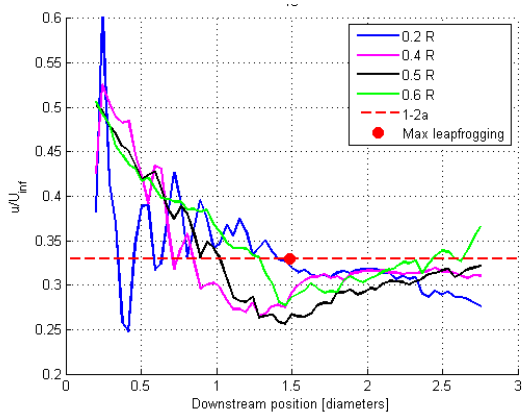

Figure 3. Streamwise profiles of normalized phase locked axial velocity field at 4 different radial locations (from [13])

Figure 4 shows the phase-average velocity and turbulence fields. It is evident how the turbulence intensity in the phase-locked field increases after the leapfrogging event.

Figure 5 shows the fluxes (see Eq.(3)) of the mean flow kinetic energy in a selected phase by action of the periodic (top) and random fluctuations (bottom). The method for separating these two contribution is explained in [15]. Positive values mean downward fluxes of kinetic energy, therefore energy entrained in the wake. Two zones can be identified. The first zone, before the vortex breakdown where the wake expansion occurs, shows the tip-vortex structures to be the only structures determining a mean flow kinetic energy transport across the wake layer, although with a negligible net value, due to both positive and negative contribution of similar magnitude. The second zone, after the wake instability and the tip vortex breakdown, is characterised by a downward net entrainment of kinetic energy, i.e. towards the inner region of the wake, caused by the random turbulent motions, signifying a dominant role of these flow structures in the re-energising process. The result is in accordance with the hypothesis of [16] who stated that the near wake tip-vortices are acting as a shield, inhibiting the wake to mix with the outer flow.

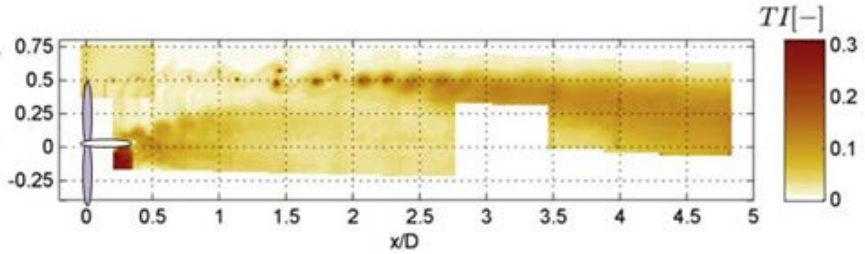

Figure 4. Unconditioned (top) and phase-locked (bottom) average turbulence intensity in the wake of the WT in the first campaign (from [13])

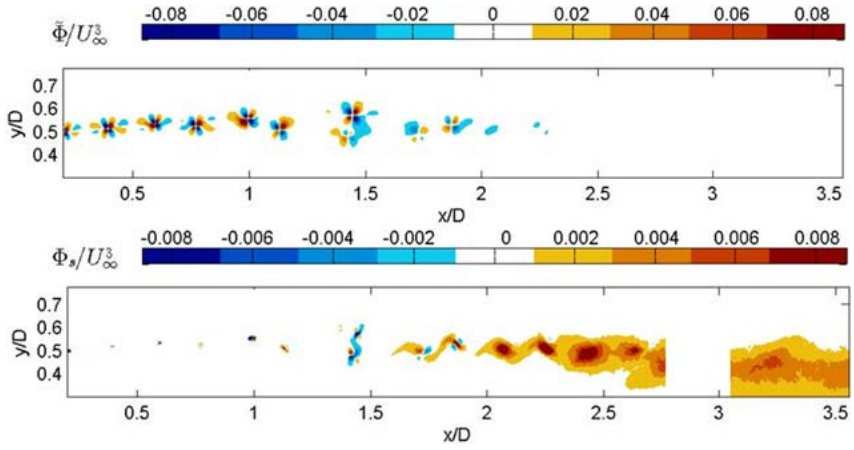

Figure 5. Mean flow kinetic energy transport due to the periodic (top) and random (bottom) fluctuations in the wake of the WT in the first campaign (from [15])

3.2 Second experimental campaign

Figure 6 show the time-average velocity field in the AD (top) and WT (bottom) wake for λ = 6.97. The presence of the leapfrogging is again visible in the localised shear layer thickness increase between *x/D* ~ 1.25 and *x/D* ~ 2. Apart from slight inhomogeneity of the flow close to the wake central axis, the two velocity field are very well comparable (see details in [14]). Larger differences between the two wakes are visible in Figure 7, which shows the time-average total turbulence intensity in the AD (top) and WT (bottom) wake. The stronger fluctuations in the WT wake are due to the presence of concentrated tip vortices. However, despite the so-calculated total turbulence intensity in the near wake of the WT is two to four times as large as the one of the AD wake, both wakes exhibit the same value of mean flow kinetic energy flux in the near-wake shear layer. This is presented in Figure 8. This quantity collapses to 50% of its original value after the breakdown of the WT's tip-vortices caused by the pairing instability. This demonstrates how the physics governing the turbulent mixing in the two wakes are intrinsically different and, as hypothesised by [16] and [8] that the presence of strong coherent fluctuations in the near wake does not enhance the wake mixing.

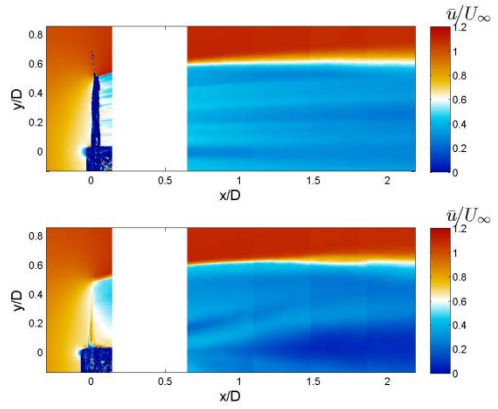

Figure 6. Unconditioned average axial velocity field in the wake of the AD (top) and of the WT (bottom) (from [15]).

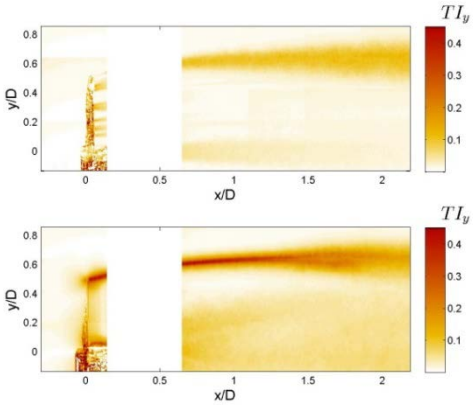

Figure 7. Unconditioned average turbulence intensity in the wake of the AD (top) and of the WT (bottom) (from [15]).

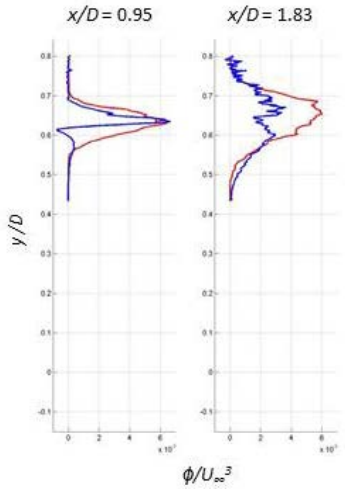

Figure 8. Mean flow kinetic energy transport at x/D = 0.95 and x/D = 1.83 (from [15]).

4 DISCUSSION AND CONCLUSIONS

The study of the time average and phase-lock average velocity fields demonstrated how the wake instability affects dramatically all of the flow properties. The leapfrogging phenomenon has a strong influence on the development of the wake turbulence, leading to a more effective mixing after the location where the instability occurs and the vortex coherence is disrupted. The general comparison between the phase-lock and the unconditioned measurements shows that the mixing process after the wake instability is solely dominated by the random motions. The peak of turbulence observed in Figure 7(bottom) is due to the presence of concentrated tip vortices. These flow fluctuations are normally accounted for in the calculation of the *added turbulence* [7, 15], which represents the flow turbulence caused by the presence of the turbine and added to the ambient turbulence [8]. This includes both coherent periodic structures, as the tip-vortices, and random velocity fluctuations, which are not separated in the classical double Reynolds decomposition applied in this work for the analysis of the second campaign. This leads to the well-known peaks of turbulence intensity close to the rotor at the blade-tip location. The analysis of the mean-flow kinetic energy transport shows clearly that the strong near-wake flow fluctuations do not contribute to the turbulent mixing, which in fact starts only after the tip-vortex breakdown. This is an issue that must be taken into account especially when validating actuator-disc based numerical models, which as shown in the second measurement campaign are characterised by a very different mixing process. As a matter of fact, the experimental comparison between the wake of a rotor and the one of a porous disc demonstrated that the physical model of the actuator disc is in principle able to reproduce the wind turbine wake velocity field correctly up to the very near wake, also in presence of very low inflow turbulence, despite what is normally believed [20]. However, the physics governing the turbulent mixing in the two wakes are intrinsically different. This project is intended to provide the basic knowledge about the different physics governing the two wake flows and, eventually, to constitute the basis for understanding the origin of the limitations of and improving the current wake models based on the actuator disc assumption.

ACKNOWLEDGMENTS

We would like to thank funding from the FLOW project. A special thanks to Dr Gerard Schepers for his collaboration and the provided information.

REFERENCES

[1] S. Aubrun, P. Devinant and G. Espana, *European Wind Energy Conference EWEC 2007*, Milan, Italy, 2007
[2] S. Aubrun, S. Loyer, P. E. Hancock and P. Hayden, *Journal of Wind Engineering and Industrial Aerodynamics*, Vol. 120, pages 1-8, 2013
[3] R. J. Barthelmie, S. T. Frandsen, M. N. Nielsen, S. C. Pryor, P. E. Rethore and H. E. Jørgensen, *Wind Energy*, Vol. 10, 6, pages 517-528, 2007
[4] H. Bolnot, T. Leweke and S. Le Dizes, *6th AIAA Theoretical Fluid Mechanics Conference*, Honolulu, Hawaii, 2011
[5] R. B. Cal, J. Lebrón, L. Castillo, H. S. Kang and C. Meneveau, *Journal of Renewable and Sustainable Energy*, Vol. 2, pages 2010
[6] B. Cantwell and D. Coles, *Journal of Fluid Mechanics*, Vol. 136, pages 321-374, 1983
[7] A. Crespo and J. Herna´ndez, *Journal of Wind Engineering and Industrial Aerodynamics*, Vol. 61, 1, pages 71-85, 1996
[8] A. Crespo, J. Hernández and S. Frandsen, *Wind Energy*, Vol. 2, 1, pages 1-24, 1999
[9] M. Felli, R. Camussi and F. Di Felice, *Journal of Fluid Mechanics*, Vol. 682, pages 5-53, 2011
[10] U. Hütter, *Annual Review of Fluid Mechanics*, Vol. 9, pages 399-419, 1977
[11] S. Ivanell, *Numerical Computations of Wind Turbine Wakes*, Royal Institute of Technology KTH - Gotland University, 2009
[12] S. Ivanell, R. Mikkelsen, J. N. Sørensen and D. Henningson, *Wind Energy*, Vol. 13, 8, pages 705-715, 2010
[13] L. E. M. Lignarolo, D. Ragni, C. Krishnaswami, Q. Chen, C. J. Simão Ferreira and G. J. W. van Bussel, *Renewable Energy*, Vol. 70, pages 31-46, 2014
[14] L. E. M. Lignarolo, D. Ragni, C. J. Simao Ferreira and G. J. W. van Bussel, *33rd ASME Wind Energy Symposium*, 2015
[15] L. E. M. Lignarolo, D. Ragni, C. J. Simão Ferreira and G. J. W. van Bussel, *32nd ASME Wind Energy Symposium*, 2014
[16] D. Medici, *Experimental Studies of Wind Turbine Wakes – Power Optimisation and Meandering*, Royal Institute of Technology (KTH), 2005
[17] F. Pierella and L. R. Sætran, *17th Australasian Fluid Mechanics Conference*, Auckland, New Zealand, 2010
[18] W. C. Reynolds and A. K. M. F. Hussain, *Journal of Fluid Mechanics*, Vol. 54, 02, pages 263-288, 1972
[19] J. Sanz Rodrigo and P. Moriarty, *TASK 31 - Benchmarking of wind farm flow models. Final Report to ExCo 74* 2014
[20] J. G. Schepers, *Engineering models in wind energy aerodynamics*, Delft University of Technology, 2012
[22] P. M. Sforza, P. Sheerin and M. Smorto, *AIAA Journal* Vol. 19, 9, pages 1101-1107, 1981
[23] J. N. Sorensen, *Journal of Fluid Mechanics*, Vol. 682, pages 1-4, 2011
[24] L. J. Vermeer, J. N. Sørensen and A. Crespo, *Progress in Aerospace Sciences*, Vol. 39, 6-7, pages 467-510, 2003
[25] P. E. J. Vermeulen, *Mixing of Simulated Wind Turbine Wakes in Turbulent Shear Flow: Report*, Hoofdgroep Maatschappelijke Technologie TNO, 1979
[26] Y.-T. Wu and F. Porté-Agel, *Boundary-Layer Meteorology*, Vol. 138, 3, pages 345-366, 2011